Half-Life Determination of ^{32}Si

J.M. Heim,[1] V.E. Barnes,[1,2] E. Fischbach,[1,2,*] D. Neff,[1] N. Cinko,[1] M. Pattermann,[1]
J.M. Nistor,[1] J.H. Jenkins,[3] T.M. Mohsinally,[1] H.B. Kaplan,[1] and P.A. Sturrock[4]

[1]*Department of Physics & Astronomy, Purdue University, West Lafayette, IN 47907 U.S.A.*
[2]*SNARE Inc., West Lafayette, IN 47906 U.S.A.*
[3]*Department of Nuclear Engineering, Texas A&M University, College Station, TX 77840 U.S.A.*
[4]*Kavli Institute for Particle Astrophysics and Cosmology and Center for Space Science and Astrophysics, Stanford University, Stanford, CA 93405 U.S.A.*

(Dated: January 14, 2020)

We report the results of a six year study of the half-life of ^{32}Si, utilizing both the original mechanical apparatus and the radioactive sources studied in an earlier experiment at Brookhaven National Laboratory (BNL). The BNL experiment was designed to mitigate the effects of systematic influences on the determination of the half-life of ^{32}Si by utilizing the ratio of counts observed for ^{32}Si to ^{36}Cl, whose half-life is 301,000 yr. We modified the system to incorporate a modern detector and electronics, which allowed us to accumulate data continuously over almost 6 year period between August 2013 and May 2019. We find for the half-life of ^{32}Si, $T_{1/2} = 162(6**)$ yr, compared to the BNL value of 174(4) yr. [????? Our results also exhibit a persistent annual oscillation in the Si/Cl ratio data, similar to, but smaller than, that observed in the BNL experiment.]

Keywords: Half-life , Si-32

Method	$T_{1/2}$ (yr)	Reference
Ice Core	330(40)	Clausen [1]
	222, 277	Clausen → Demaster [2]
Sedimentary Core	276(32)	Demaster [2]
	217(29)	Demaster → Cumming [3]
AMS	101(18)	Kutschera et al. [4]
	108(18)	Elmore et al. [5]
	132(13)	Chen et al. [6]
Activity + AMS	133(9)	Hofmann et al. [7]
	162(12)	Thomsen et al. [8]
Direct Decay Measurement	172(4)	Alburger et al. [9]
	159(6)	This Work

TABLE I. Summary of half-life determinations for ^{32}Si, grouped by method.

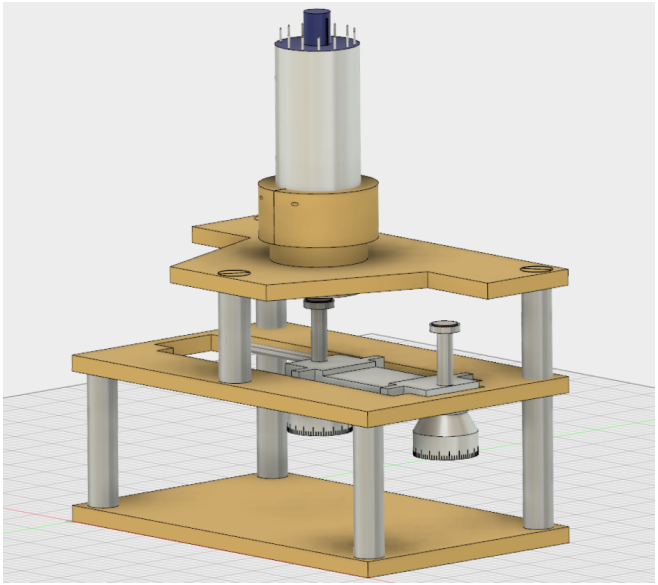

FIG. 1. Illustration of the sample changer geometry including the new detector mount, added for this work.

I. INTRODUCTION

Recent determinations of the half-life of ^{32}Si have produced a number of discrepant results, with laboratory-based experiments yielding results between 101(8) yr to 172(4) yr (see Table I). Since SiO_2 is widely distributed in the environment, ^{32}Si generated by cosmic radiation can be used as a radioactive tracer in various geophysical applications, given an accurate determination of its half-life. However, the range of reported determinations in Table I makes it clear that further study is warranted. The half-life determination in this work is a result of a study aimed at understanding the apparent oscillatory behavior in the ^{32}Si decay rate observed by Alburger, Harbottle, and Norton [9] in their half-life determination carried out at Brookhaven National Laboratory (BNL). Our efforts were greatly facilitated by the BNL group, who graciously provided their original apparatus and radioisotope samples to us. The custom built sample changer (See Figure 1) allowed the decay rate of ^{32}Si to be continuously compared to the long-lived ^{36}Cl reference. As described below, we adapted the sample changer to a new detector and updated the associated electronics while also recording the environmental conditions in the laboratory, which might affect the stability of the detection system.

In the following sections, we describe the changes made to the original BNL counting apparatus, characterizations of system response to various environmental

* Corresponding Author: ephraim@purdue.edu

changes, the detailed data acquisition protocol, our half-life determination of ^{32}Si, and a summary of our results compared to other determinations.

II. DESCRIPTION OF SYSTEM

As noted above, our half-life determination of ^{32}Si utilized the original ^{32}Si and ^{36}Cl samples as well as the sample changer used in the earlier study at BNL [9]. The original apparatus was modified to include a collar designed to mount our detector, sensors for confirmation of sample positioning, and air snubbers to dampen the seating of the pneumatically driven sample cart as it approached either end of the rails. Additionally, we built a modern data acquisition (DAQ) system including more robust environmental control and extensive data logging. The sample changer was placed in a modified steel drum and kept at a controlled pressure with high-purity nitrogen, which allowed us to also minimize variations in relative humidity. The DAQ system consisted of a 2-inch diameter 0.010-inch thick Bicron plastic scintillation detector near the window of a 10-stage photomultiplier tube coupled to an ORTEC 276 preamplifier base. A NIM-based spectroscopy amplifier [model, make] and multichannel analyzer (MCA) [model,make] connected to a PC running Maestro32 and custom LabVIEW software completed the core DAQ system. The sample changer alternated between the long-lived ^{36}Cl and the ^{32}Si every 30 minutes during a given run. This frequent interleaving of ^{36}Cl and ^{32}Si observations was designed to reduce the effect of systematics by utilizing ratios of sample counts which are quasi-coincident in time.

III. COUNTING PROCEDURE

The ^{32}Si and ^{36}Cl samples were placed on the symmetric, micrometer-adjustable source holders in the sample changer and positioned (2.00 ± 0.02) mm from the face of the detector and locked in place A piston driven with nitrogen gas shuttles the source alternately into place under the detector, automatically when requested by the DAQ software. Once a sample-position-sensing microswitch is activated, an 1800 s live-time collection of the energy spectrum begins. A typical spectrum for each source is illustrated in Figure 2. Each run of 200 cycles is followed by a 30 minute collection of the background counting rate, typically 0.78 Hz, with a RMS variation of 3% , consistent with statistical fluctuations of the 1400 counts per half-hour collection time. This compares to count rates of $\approx$ 100 Hz and 200 Hz for the ^{32}Si and ^{36}Cl, respectively.

IV. SCALING ALGORITHM

The energy spectra of the two radionuclides are shown in Figure 2. For each isotope, counts are taken within defined Regions of Interest (ROI). Clearly, gain shifts will move counts into one side of a ROI and out of the opposite side of the ROI, and generally the counts per channel are different at the opposite ROI edges. Hence a shift in gain will in general lead to a systematic shift in recorded counting rate. Gain corrections are relatively easy to do when counting gamma rays, provided there are reasonably narrow identifiable peaks in the energy spectrum. There is no such feature in the present energy spectra, but it has proved possible to exploit the one "crisp" feature of the spectra, namely the sharp rise in the general vicinity of bin 100. A set of spectra collected for a few days near the beginning of the measurements, and while the gain was nominally constant, are averaged together to produce an archetype ROOT histogram object. For all subsequent spectra, we use an "accordion scaling" algorithm which stretches or compresses the spectrum and distributes fractions of old bin contents into a new 1024 bin spectrum. These scaled spectra are compared with the archetype, and the scaling parameter is varied to minimize the chi-squared deviation of the spectrum relative to the archetype, summed over a range of about a dozen bins in the region of the sharp rise. The gain-scaled spectra are found to conform to the archetype over the entire 1024-bin spectral range. This procedure is somewhat analogous to the electronic gain stabilization which is routinely applied to gamma spectra. The software gain stabilization is essential to this experiment, since the HV supply tended to drift with time, with attendant gain shifts. The HV was periodically readjusted to a nominal value of 950 V, to keep the shifts within bounds. Even at fixed voltage, there was a slow secular drift upwards of the gain. At one point the HV setpoint was dropped to 935 V, to restore the gain to the original value at the time of the archetype. It will be seen, with very high resolution, in the de-trended counting rate plots that the various steps in gain from HV adjustments do not cause steps in the data. Another (much less sensitive) example of the efficacy of the gain-scaling algorithm can be seen by comparing the scaled and non-scaled data in Figures 9 - 12. The relationship between the computed gain-scaling parameters and the detector voltage is also shown in Figure 13. The gain-scaling parameters track the detector voltage, as expected, with the gain varying approximately as $V^{8.5}$ which is reasonable for a typical 10-stage photomultiplier tube.

V. SYSTEMATIC EFFECTS

Other sources of counting error, in addition to uncorrected gain shifts, include possible deadtme and pileup effects, which are rate dependent and are expected to be negligible at the very low counting rates in this ex-

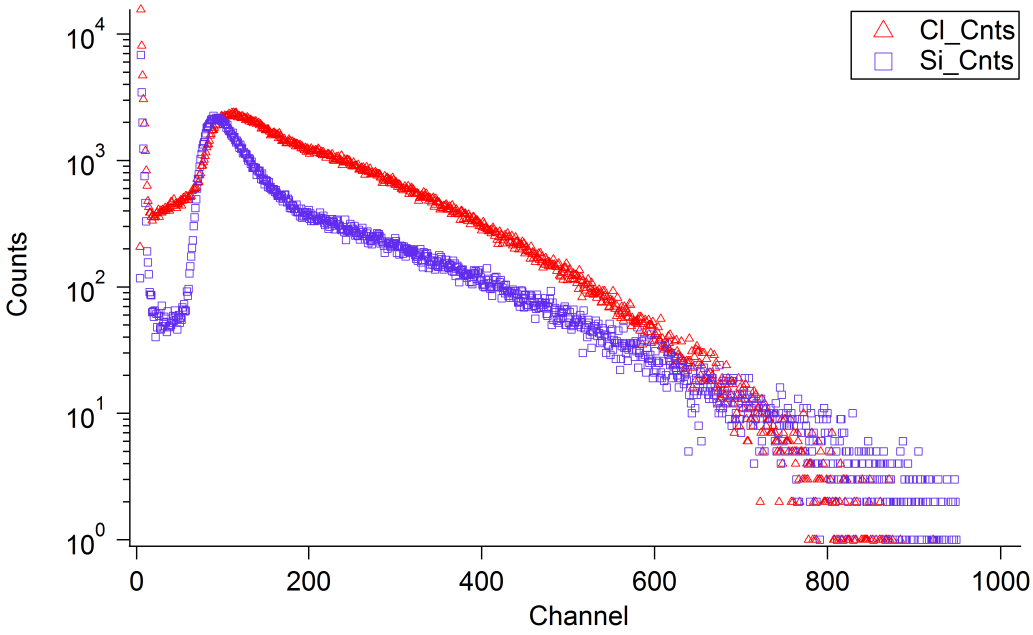

FIG. 2. Representative Si (lower) and Cl (upper) energy spectra with shaded statistical error bands.

periment. Furthermore, the counting rate for the ^{36}Cl is effectively constant, and the rate for the ^{32}Si has dropped by only 3.6% over the duration of this experiment, so be believe that variations, if any, in pileup and deadtime will have negligible effects on fitted half-lives.

The remaining source of counting error would be geometric, that is, changes in solid angle subtended by the detector if the source does not return exactly to the same position relative to the detector on each cycle. The BNL source carriage has precision rails and well-defined end-stops. Tight temperature control of the system is designed to minimize any possible effects of differential thermal expansion. Furthermore, the horizontal brass plates of the apparatus are separated by vertical steel posts, which almost match the heights of the steel micrometer shafts supporting the two sources. Control of the pressure around the apparatus is designed to prevent any mechanical motions such as, for example, of the thin window between the sources and the plastic scintillator.

Data were recorded for temperature, absolute pressure, relative humidity, magnetic field, line voltage, and high voltage over the course of the experiment. Temperature, relative humidity, and pressure were measured every 60 s by a NIST traceable data logger (TR-73U by T&D Corp.), and processed in the system control software. Based on the pressure reading, the PC actuated a relay which opened or closed a valve controlling the flow of nitrogen into the drum (there is a very slow leakage of Nitrogen from the drum.) The magnetic field was monitored with a 12-bit 3-axis magnetometer (Honeywell HMC5883L), while the line voltage and high voltage were recorded with a 14-bit precision ADC (Measurement Computing 1408FS). The variation in daily mean temperature in the room was typically less than $\pm 2\,^{\circ}$C. The recorded pressure data inside the drum indicate stability to a few tenths of an hPa, apart from a few intermittent deviations. Similarly, the %RH (relative humidity) inside the drum was stable to better than $\pm 1\%$ at almost all times. Typical variations in the observed magnetic field were less than 10 mG, although we witnessed an apparent shift in the baseline magnitude on the order of 50 mG. This was primarily in the the longitudinal components, while only the axial component was shown to be significant in affecting detector response at a field strength of 4.6 Gauss (and not at 2 Gauss.) Even if the above-mentioned change in the magnetic field had been along the detector axis, it was a factor of 20 below the level shown to be a safe region of operation. Given the step-wise nature of this change, it is possible that the (inaccessible) sensor inside the drum shifted in orientation. The line voltage varied between 115 and 119 V, which falls well within the bounds of stability shown by our characterization of the system, discussed earlier. The high voltage (HV) slowly drifted upward, and every few days was manually corrected back to a nominal 950 V using a Fluke DVM. The gain-scaling parameter tracked this saw-toothed pattern of HV changes, but there was also slower HV-independent increase in gain with time. which later accelerated suddenly, going from a relative gain of 1.10 to 1.15 in a short period of time. At that point we established a new HV set-point of 936 V, with continuing periodic manual HV readjustments. As previously discussed, we applied the gain-scaling algorithm to correct for all gain variations from any source. As

mentioned earlier, and visible in Figs X and Y, after gain correction, the high-resolution exponentially de-trended Si and Cl data show no sign of sharp changes when there are sharp changes in the HV (and hence gain).

VI. HALF-LIFE DETERMINATION

Between August 2013 and May 2019, approximately 7×10^9 ^{32}Si decays and 14×10^9 ^{36}Cl decays were recorded. As previously noted, the samples were observed alternately: the data points for ^{36}Cl and ^{32}Si are interleaved at 30-minute counting intervals. In determining the half-life of ^{32}Si, the ratio of ^{32}Si/^{36}Cl was analyzed in an attempt to suppress systematic effects. In the following analysis of the ^{32}Si half-life, systematic errors are determined from the characterization data presented above. Although the gain-scaling algorithm discussed in section 3.1 [was shown to mitigate] the effects due to gain shifts to within the statistical error bars, we quote the contribution of HV (and other gain-related) systematic uncertainty as being equal to the size of the statistical uncertainty of each datum. [*****The increased spread observed in the ^{32}Si characterization data, during and after the temperature changes, motivated an additional increase of $1\sigma_{stat}$ in reported systematic uncertainty.(VERY LOW STATISTICS short-term data, weak indication of anything– kill this wording and this contribution to uncertainty – then redo the weighted fits NEED JORDAN'S NIFTY WEIGHTED FITTING PROGRAM(S) *******] An unexplained month-long increase in ^{36}Cl counts between February and March 2014 resulted in a small but significant decrease in the ratio data, which were removed from this analysis. Additionally, a small number of outliers produced on days for which only a few 30-minute cycles were collected, were also excluded.

The background data to be subtracted were gain-scaled not using features of the background spectrum, but rather using the gain scaling parameter of the nearest isotope measurement. The gain-scaled background measurements are plotted in *NEWFIG* and are a nearly constant 1400 counts per half hour period over the duration of the experiment, with a RMS variance of 46 counts (cf. the Gaussian σ of 67 counts.) The background subtracted from each source point was interpolated between the nearest-in-time flanking backgound measurements.

The backgrounds were subtracted propagating statistical uncertainties. The background-subtracted data were combined into daily mean ^{32}Si/^{36}Cl ratios [mean Si / mean Cl, or mean of a number of ratios? how were the number of Si points and Cl points equalized ?] and fit with a purely exponential function (see Eq. 1), weighted by total statistical and systematic uncertainties (see Figure 5). The half-life determination of this fit yields $T_{1/2} = 161.8$ yr $\pm$ 1.7 yr (statistical) $\pm$ 3.3 yr (systematic) with $\chi^2_{DOF} = 1.07$, which agrees well with Thomsen's determination [8]. The residuals of this fit and the associated histogram are presented in Figures 6 and 7, respectively. [why are these figures named CosFit? does this imply adding in a cos(wt) term???]

$$f(t) = Ae^{-\lambda t} \tag{1}$$

where A is the amplitude, λ is the decay constant, and t is time. The fitting procedure weights each datum by the associated uncertainty and utilizes the Levenberg — Marquardt algorithm, which minimizes χ^2, defined by,

$$\chi^2 = \sum_{i=1}^{N} \frac{1}{\delta M_i^2} \left[M_i - f\left(t_i; A, \lambda\right)\right]^2 \tag{2}$$

where N is the number of data points, M_i is the i^{th} datum with uncertainty δM_i, t_i, is the time associated with the i^{th} datum, A is the amplitude, and λ is the decay constant. Utilizing the period and phase from a cosine fit applied to the residuals of the exponential best-fit to the data (Figure 6), we apply a combined exponential+cosine function (Eq. 3) with the aim of removing the effect of a possible non-integer number of oscillatory cycles on the half-life determination (See Figure 8).

$$F(t) = Ae^{(-\lambda t)}(1 + Bcos(\omega t + \phi)) \tag{3}$$

The result is $T_{1/2} = 159.4$ yr $\pm$ 1.9 yr (statistical) $\pm$ 3.7 yr (systematic) with$\chi^2_{DOF} = 1.01$. As indicated in Figure 8, the amplitude of modulation observed in our Si/Cl ratio data is $2.1 \pm 1.1 \times 10^{-4}$, which is not statistically significant. The original BNL experiment reported an oscillation with considerably larger amplitude of 1.5×10^{-3}; however a subsequent reanalysis of the BNL data by Sturrock et. al. [10] found reduced oscillation amplitudes of the two [samples — do you mean sources????]. A broader analysis of the observed oscillatory behavior is presented in [11]. The phase of the possible annual oscillation puts the peak at about [February XX ??] [cf. the BNL phase, is ours maybe close to the same?]

VII. SUMMARY

^{32}Si half-life determinations from various experiments are listed in Table I, exhibiting a clear lack of consensus. The grouping of determined values by method, suggests that the discrepancies are of systematic origin, though we note that our determination is consistent with Thomsen's AMS + activity result [8], which differs from the other AMS determinations significantly. The 2σ discrepancy between our determination and that of the BNL experiment is possibly explained by the unknown contribution of their background activity during their experiment or by other unidentified systematic effects. A significant improvement to temperature control has been implemented by way of the aforementioned thermoelectric unit, and based on previous experience, we expect

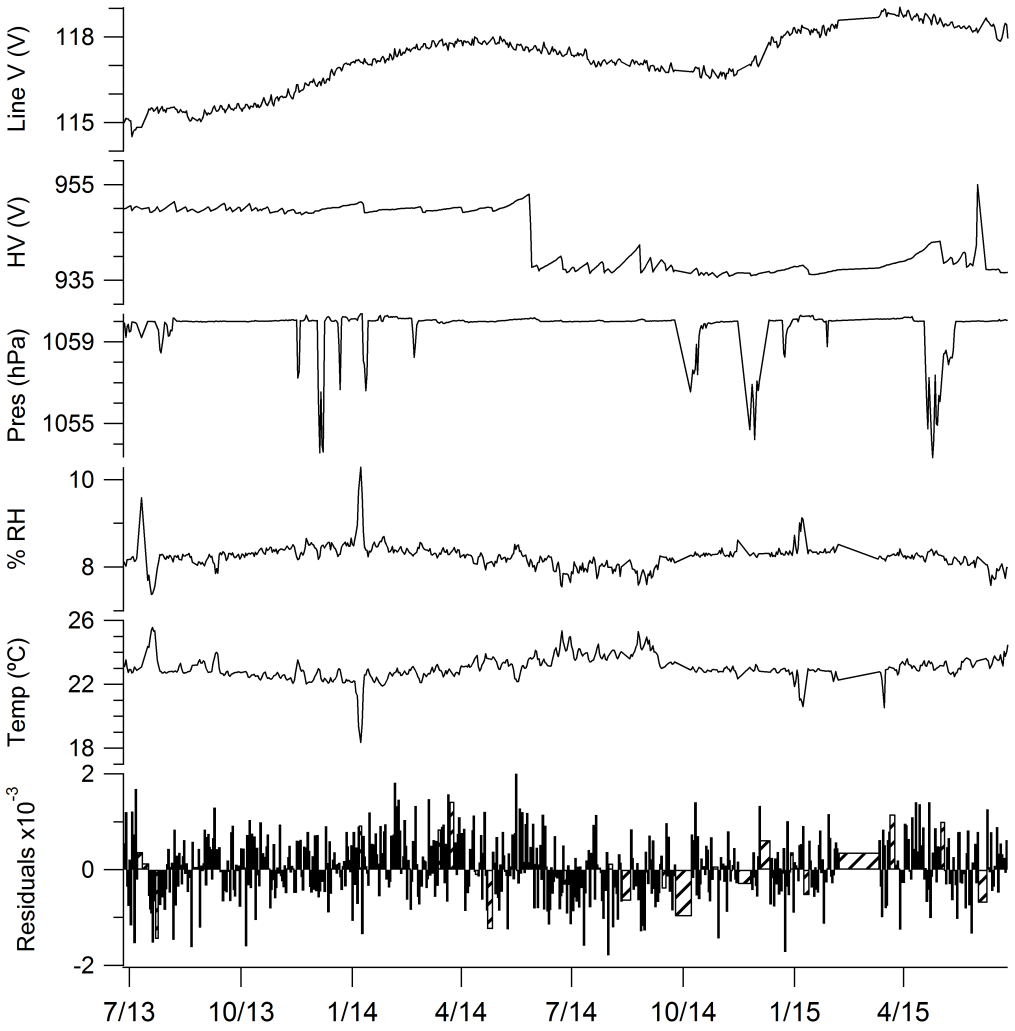

FIG. 3. Daily mean values of decay ratio residuals and environmental observations. Approximately 5×10^6 environmental readings have been logged collectively.

to achieve temperature stability of approximately 0.1 °C over extended time periods. We have also implemented daily background measurements and [are addressing the HV stability] since the HV supply was replaced on DATE, the HV has been stable to < 1 V (??).

Given the relatively long half-lives of ^{32}Si and ^{36}Cl, much can be learned from our continuing experiment using the same samples and detector system, while improving further the possible sources of systematic effects. Our results exhibit, at the two standard deviation level, a similar oscillation as observed in [9], but at an order of magnitude smaller amplitude than described in the original BNL report, which may be a result of tighter control over the local environment in the present measurements. Our future data, collected under much tighter temperature control and other improvements, could indicate to what extent such systematics are responsible for the oscillation suggested or observed in the experiments.

Appendix A: Measurements of Environmental Effects

Several tests were performed on the system in order to measure its dependence on changing environmental conditions. The detector was placed in various orientations relative to a controllable magnetic field produced by a set of Helmholtz coils. The detector response was evaluated in magnetic fields of 2 Gauss and 4.6 Gauss in axial and perpendicular orientations (relative to the detector axis), and the ^{36}Cl sample was monitored for changing count rates and spectral peak position. At 2 Gauss (4 times the Earth's magnetic field), no statistically significant change in count rate or peak position was found, but at 4.6 Gauss, a small shift in peak position was observed for the case where the magnetic field was oriented axially relative to the detector. However, at no time did the ambient magnetic field approach this value.

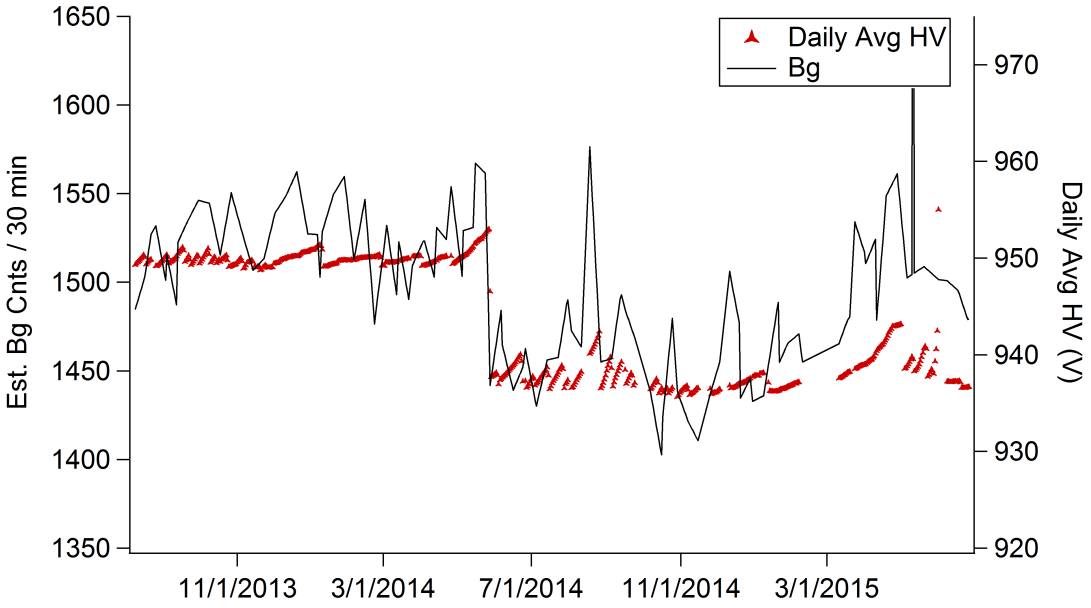

FIG. 4. Daily average HV records overlayed with manually estimated background activity suggests that the variation in the observed background is driven by the detector voltage (HV).

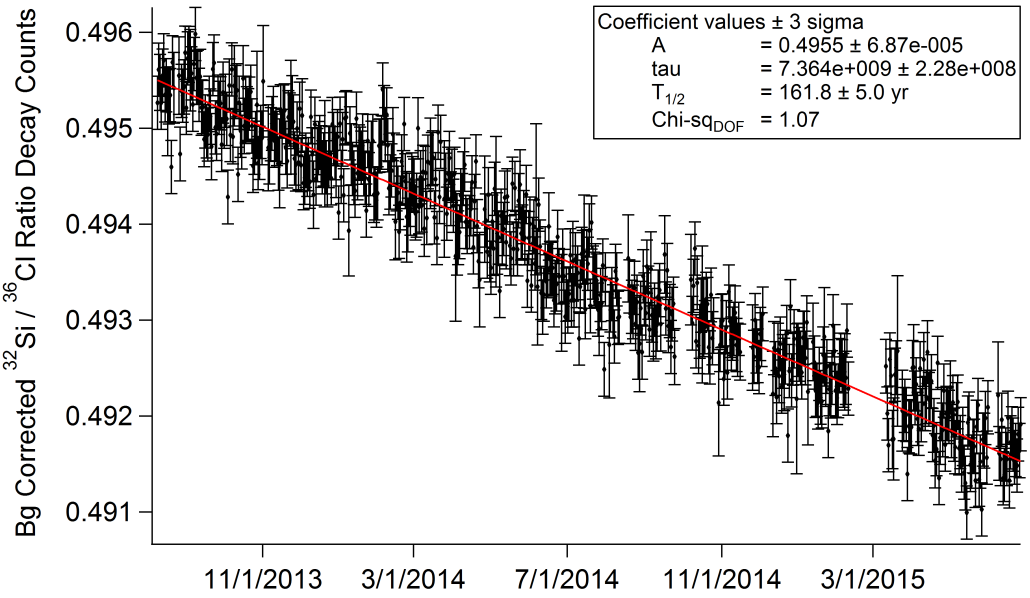

FIG. 5. Exponential fit to the background-corrected Si/Cl ratio decay data yields $T_{1/2}$ = 161.8yr ± 1.7 yr (statistical) ± 3.3 yr (systematic) with $\chi^2_{DOF} = 1.07$.

The DAQ system and high voltage (HV) supply were powered by a constant voltage transformer, whose output is nominally 117 VAC, in order to suppress possible effects from fluctuating line voltage. The HV output was found to change by less than 0.1 V for an input ranging from 109 to 125 volts. The output only began to drop when the input was decreased to 92.1 V. The NIM bin DAQ electronics, whose specifications require 103 - 129 V, were also tested in the same range of applied voltage and found to be stable to better than one [channel ???? what is a "channel"] in detector gain.

Early studies showed that the output of the HV supply

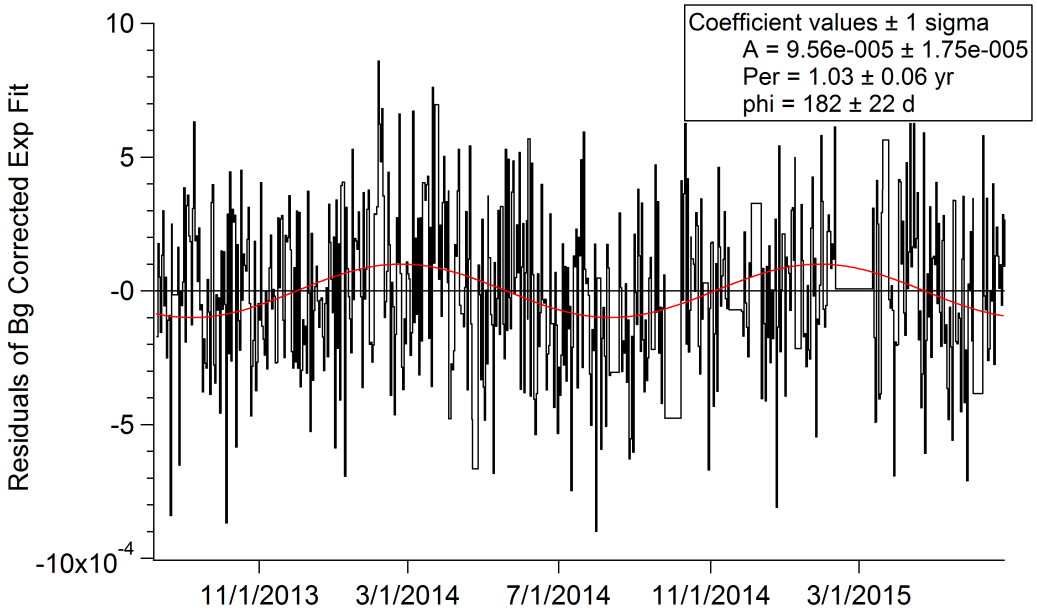

FIG. 6. Residuals of the purely exponential fit in Eq. 1 to the background-corrected ^{32}Si/^{36}Cl ratio data, fit with a cosine function.

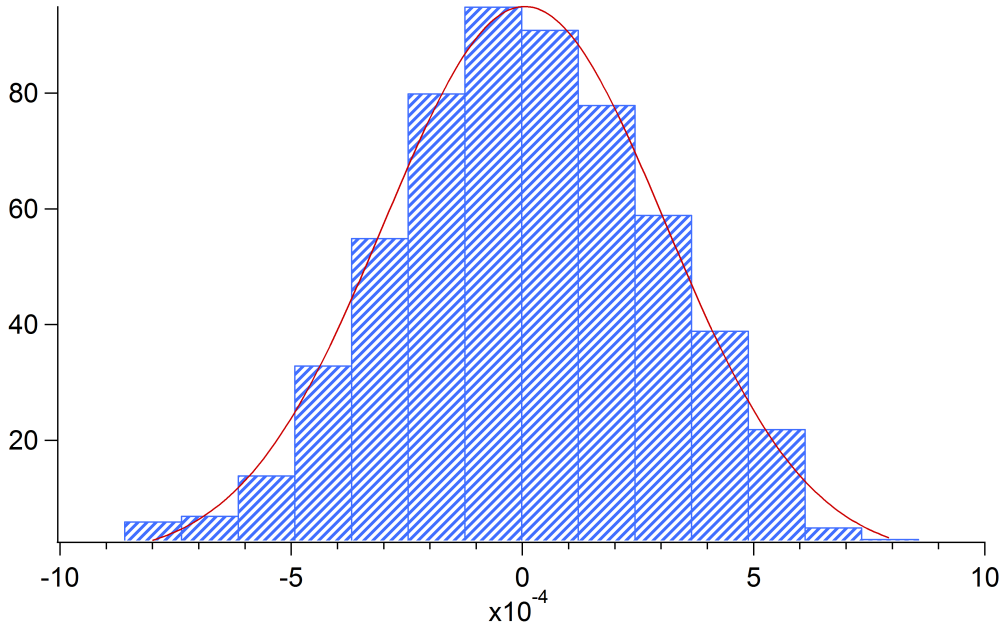

FIG. 7. Histogram of the residuals of the cosine fit in Figure 6.

varied with temperature at 0.8 channels/ °C. [Channels of what?????] The recent addition of a thermoelectric temperature control system (TECA Corp.) has allowed us to more precisely measure the system's dependence on both temperature and HV while isolating the HV supply from the rest of the DAQ components and the detector. The detector with PMT and NIM bin were characterized by incrementing the temperature of their enclosure 1 °C at a time, between 21 °C and 25 °C and recording the decay spectra. Separately, the dependence on detector voltage was quantified by changing the HV in 5 V increments while holding the temperature of these components con-

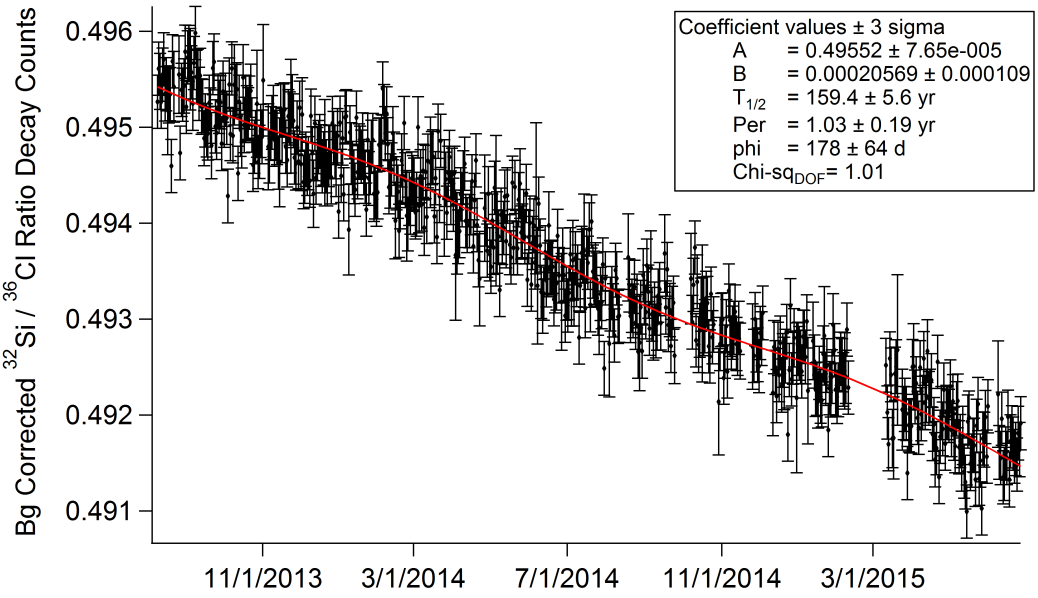

FIG. 8. The combined exponential+cosine function 3 fit to the background-corrected ratio decay data yields $T_{1/2}$ = 159.4 yr ± 1.9 yr (statistical) ± 3.7 yr (systematic) with $\chi^2_{DOF} = 1.01$.

stant. The observed counts per 30-minute interval for both ^{32}Si and ^{36}Cl are shown in Figures 9 - 12. The raw counts reflect the effects of gain shifts, which move the spectra relative to the fixed ROI counting boundaries; the scaled points have been gain-corrected, in software, by a scaling procedure to be described be, low.

Although determining the ratio of ^{32}Si to ^{36}Cl largely mitigates systematic effects, the somewhat different energy spectra of the two samples respond to changes in detector voltage differently, given the placements of the low and high ROI boundaries at channels 50 and 800 of the spectra. An increase in voltage brings fractionally more low-energy counts into the integration region for ^{36}Cl than are removed at the upper end. The opposite is true for ^{32}Si, so the net effect is different in magnitude as well as opposite in direction. The ^{36}Cl count rate shows a fractional dependence on detector voltage of approximately 2.4×10^{-4}/V, while the ^{32}Si count rate varies by approximately -1.6×10^{-4}/V. In order to correct for these effects, a very effective gain stabilizing algorithm, discussed in the next section, was developed. The effect of temperature variations on the detector and DAQ system is much smaller. The ^{36}Cl data show no obvious thermal effect, and the scatter of the data points is consistent with Gaussian statistics. The ^{32}Si data show no obvious trend as a function of temperature, but do have an RMS scatter of 0.46% while the Gaussian uncertainty on each data point is 0.22%. The difference is not statistically significant, however. In order to ensure that no solid angle changes due to placement occurred while characterizing for temperature and HV, the ^{36}Cl data were taken, without moving the carriage, while increasing either of the parameters, and the ^{32}Si data were collected, without moving the carriage, while bringing them back down. On the other hand, the sources were shuttled back and forth, in the normal manner, while holding the temperature and HV constant, to evaluate any positioning inconsistencies. ?????? what figure shows this??? leaves open the possibility of a small variation in sample placement under the detector. This effect is included [how????]in the systematic uncertainty determination. [[this discussion is somewhat problematic, we need to discuss the reasoning — also, the shuttle was NOT moved for Fig 5, was it?]]

1. Scaling Algorithm

A gain-scaling procedure was developed to correct for gain shifts. It exploits the only "crisp" feature of the spectra, namely the sharp rise in the general vicinity of bin 100, see Figure 2. Note that the spectral shapes are distorted relative to three body phase space, presumably by varying angles of the electrons entering different radial regions of the thin plastic scintillator, and ionization energy loss rate variation as a function of electron energy. A set of spectra collected for a few days near the beginning of the measurements, and while the gain was nominally constant, are averaged together to produce an archetype ROOT histogram object. For all subsequent spectra, we use an "accordion scaling" algorithm which stretches or compresses the spectrum and distributes fractions of old

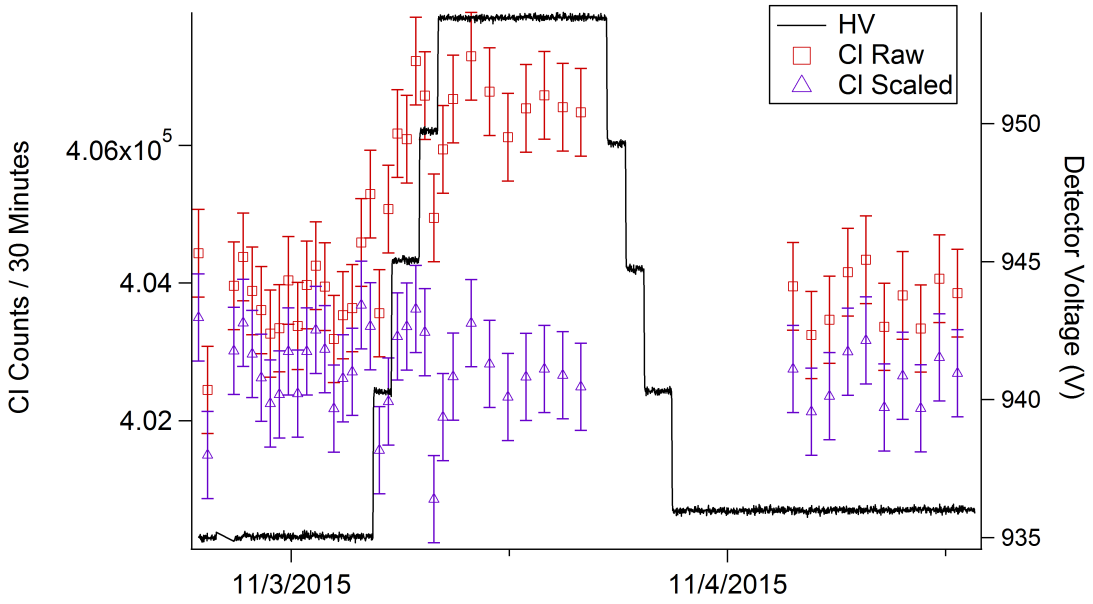

FIG. 9. 30-minute raw and scaled ^{36}Cl counts (left axis) while changing the detector voltage (right axis). A scaling procedure, which is effectively a software stabilization of the detector gain, is discussed in the text.

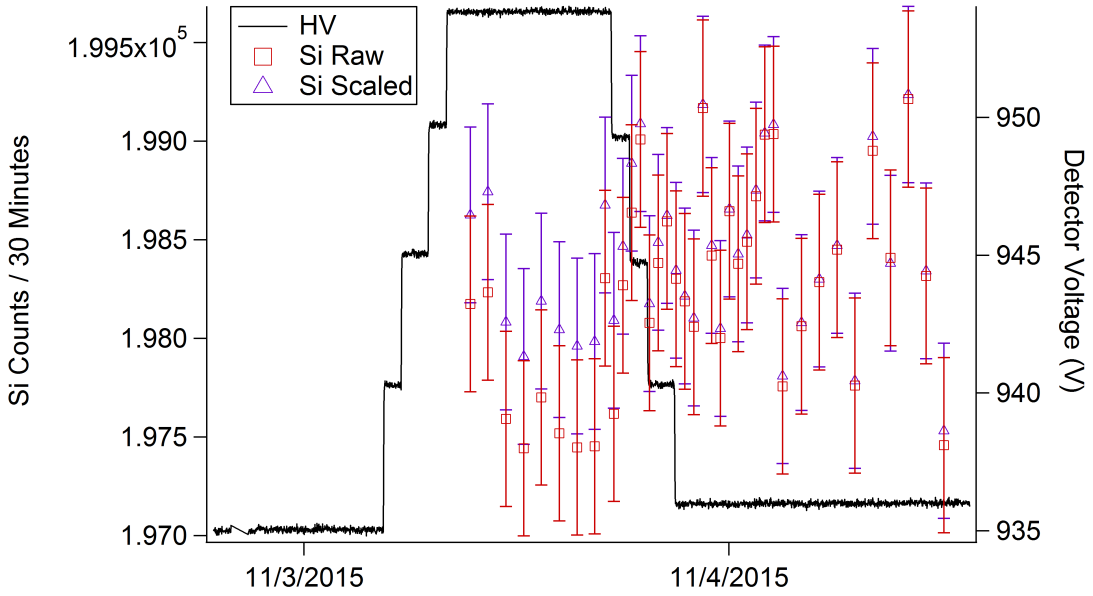

FIG. 10. 30-minute raw and scaled ^{32}Si counts while changing the detector voltage. See also caption to Figure 9.

bin contents into a new 1024 bin spectrum. These scaled spectra are compared with the archetype, and the scaling parameter is varied to minimize the chi-squared deviation of the spectrum relative to the archetype, summed over a range of about a dozen bins in the region of the sharp rise. The gain-scaled spectra are found to conform to the archetype over the entire 1024-bin spectral range [*****this needs study and confirmation.] This procedure is somewhat analogous to the electronic gain stabilization which is routinely applied to gamma spectra, where there is a well-defined peak (which is not present in a direct beta energy spectrum.) The software gain stabilization is essential to this experiment, since the HV supply tended to drift with time, with attendant gain

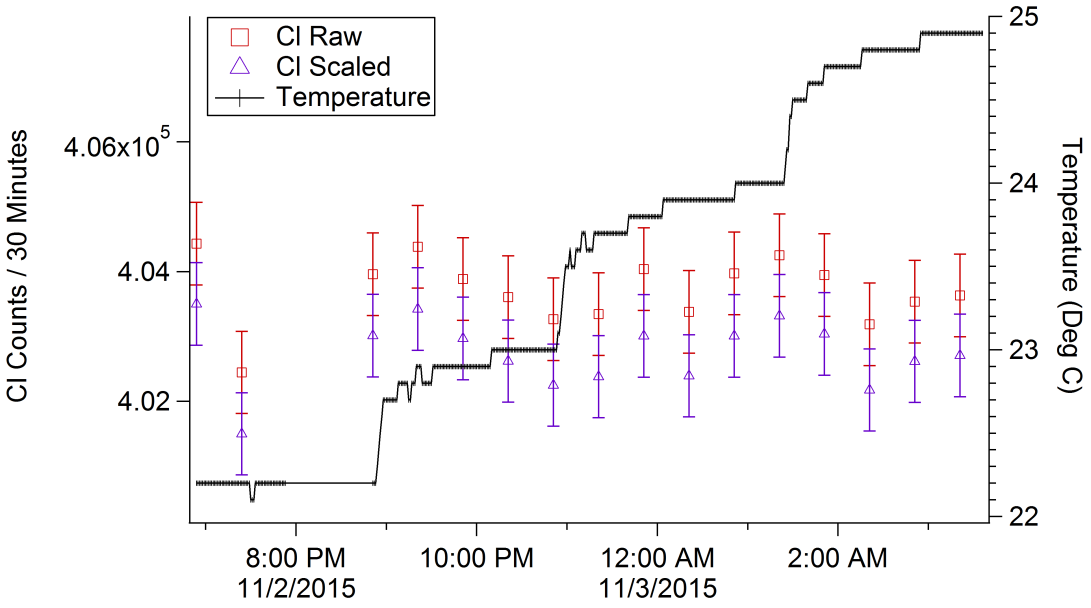

FIG. 11. 30-minute raw and scaled ^{36}Cl counts while changing the temperature of the detector and NIM bin electronics. See also caption to Figure 9.

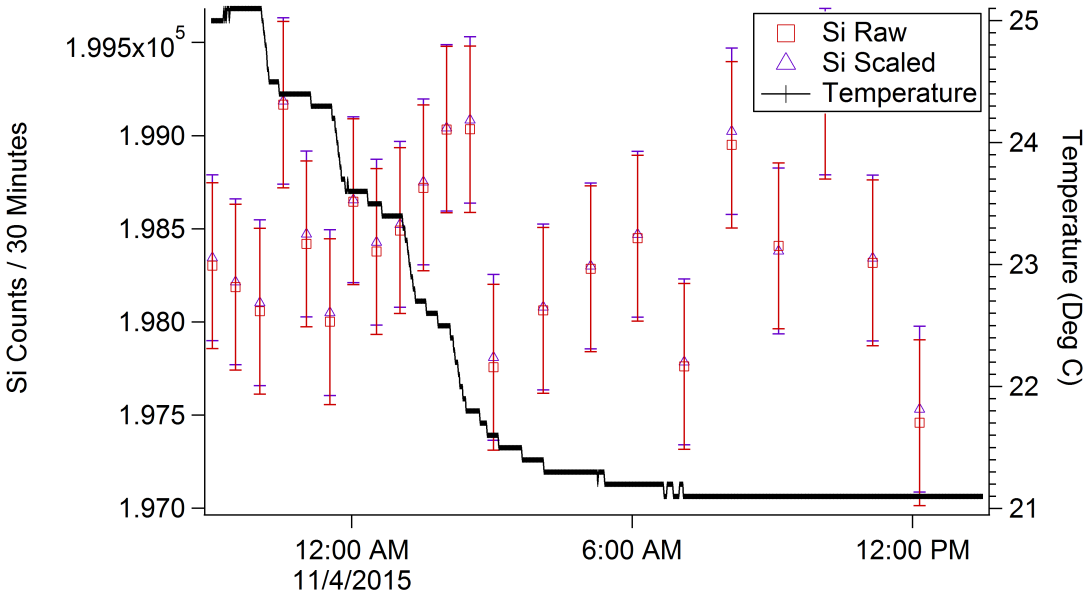

FIG. 12. 30-minute raw and scaled ^{32}Si counts while changing the temperature of the detector and NIM bin electronics. See also caption to Figure 9.

shifts. The HV was periodically readjusted to a nominal value of 950 V, to keep the shifts within bounds. Even at fixed voltage, there was a slot secular drift upwards of the gain. At one point the HV setpoint was dropped to 935 V, to restore the gain to the original value at the time of the archetype. It will be seen, with high resolution, in the de-trended counting rate plots that the various steps in gain from HV adjustments do not cause steps in the data. Another (less sensitive) example of the efficacy of the gain-scaling algorithm can be seen by comparing

the scaled and non-scaled data in Figures 9 - 12. The relationship between the computed gain-scaling parameters and the detector voltage is also shown in Figure 13. The gain-scaling parameters track the detector voltage, as expected, with the gain varying approximately as $V^{8.5}$ which is reasonable for a typical 10-stage photomultiplier tube.

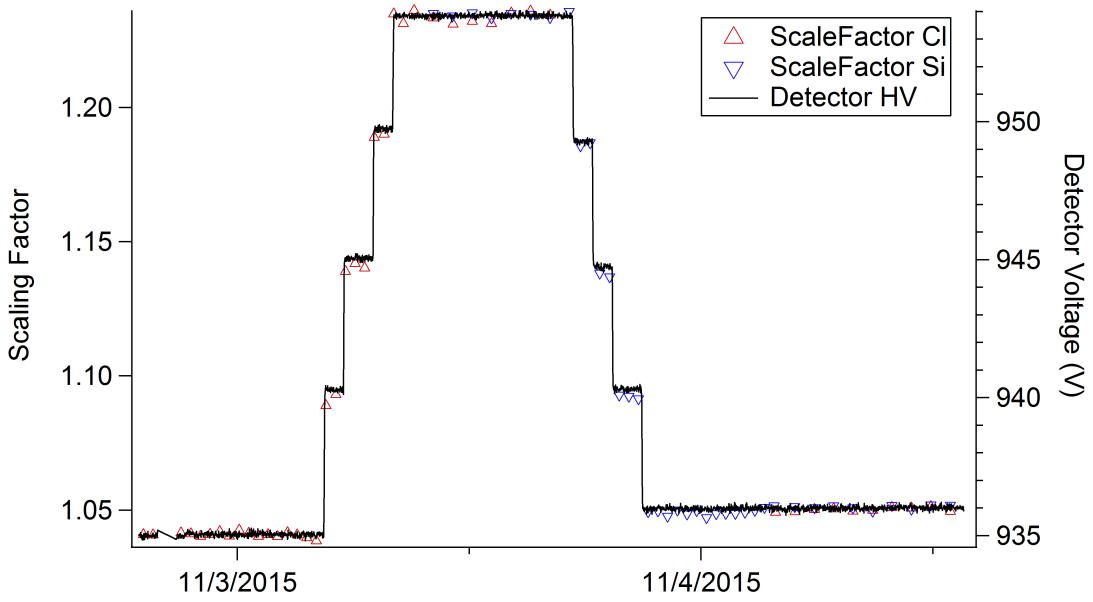

FIG. 13. Computed scaling parameters overlayed on the recorded detector voltage during characterization. See text for further details.

[1] H. B. Clausen, Journal of Glaciology **12**, 411 (1973).

[2] D. J. Demaster, Earth and Planetary Science Letters **48**, 209 (1980).

[3] J. Cumming, Radiochemical and Radioanalytical Letters **58**, 297 (1983).

[4] W. Kutschera and M. Paul, Annual Review of Nuclear and Particle Science **40**, 411 (1990), http://dx.doi.org/10.1146/annurev.ns.40.120190.002211.

[5] D. Elmore, N. Anantaraman, H. W. Fulbright, H. E. Gove, H. S. Hans, K. Nishiizumi, M. T. Murrell, and M. Honda, Phys. Rev. Lett. **45**, 589 (1980).

[6] Y. Chen, E. Kashy, D. Bazin, W. Benenson, D. J. Morrissey, N. A. Orr, B. M. Sherrill, J. A. Winger, B. Young, and J. Yurkon, Phys. Rev. C **47**, 1462 (1993).

[7] H. Hofmann, G. Bonani, M. Suter, W. Wölfli, D. Zimmermann, and H. von Gunten, Nuclear Instruments and Methods in Physics Research Section B: Beam Interactions with Materials and Atoms **52**, 544 (1990).

[8] M. Thomsen, J. Heinemeier, P. Hornshøj, H. Nielsen, and N. Rud, Nuclear Physics A **534**, 327 (1991).

[9] D. A. et al., Earth and Planetary Science Letters **78**, 168 (1986).

[10] P. A. Sturrock, J. B. Buncher, E. Fischbach, D. J. ii, J. H. Jenkins, and J. J. Mattes, The Astrophysical Journal **737**, 65 (2011).

[11] J. M. Heim, ProQuest Dissertations & Theses Global (1781664360) (2015).